Journal of Chromatography, 627 (1992) 23–35
Elsevier Science Publishers B.V., Amsterdam

CHROM. 24 549

Rapid breakthrough measurement of void volume for field-flow fractionation channels

J. Calvin Giddings, P. Stephen Williams and Maria Anna Benincasa*

Field-Flow Fractionation Research Center, Department of Chemistry, University of Utah, Salt Lake City, UT 84112 (USA)

(First received May 4th, 1992; revised manuscript received August 5th, 1992)

ABSTRACT

A peak breakthrough technique is described and evaluated for measuring the void volume of field-flow fractionation (FFF) channels, particularly those used for flow FFF. This technique uses a high-molecular-mass macromolecular or particulate probe that can be displaced rapidly by flow through the FFF channel with minimal transverse diffusion. The particles that emerge first are those carried through the entire length near the channel centerline at the apex of the parabolic flow profile. These particles generate a sharp breakthrough profile. The measured breakthrough time is two thirds of the void time, thus making it possible to calculate both the void time and the associated void volume. This method, although applicable to all FFF channels (and capable of extension to open tubes), is particularly useful for flow FFF because conventional low-molecular-mass void probes can diffuse into the permeable walls and thus distort void measurements. The theoretical basis of the breakthrough technique and an explanation for the sharpness of the breakthrough front are given. A method for compensating for deviations from perfect sharpness is developed in which the breakthrough time is identified with the time needed to reach 85–88% of the breakthrough peak maximum. Preliminary experimental results are shown using various protein probes in four different FFF channel systems.

INTRODUCTION

The void volume V^0 (or, equivalently, the void time t^0) is a critical parameter in field-flow fractionation (FFF) whose value must be established in order to derive molecular mass and particle size information from FFF retention measurements [1–4]. In principle, V^0 and t^0 are simple to measure: they can be equated to the experimental retention volume and time, respectively, of a component that is unaffected by applied external fields. Such a component will ordinarily be distributed fairly evenly over the channel cross-section and its observed average velocity will equal the mean velocity of the carrier fluid in the FFF channel. The component should thus emerge from the channel (and be detected) after a volume of carrier approximately equal to the volume of the empty space, or void volume, is displaced through the channel. Hence V^0 should be obtainable in two ways: either as the measured "sweep" or "retention" volume of a non-retained component peak or as the physical volume of the FFF channel. As FFF channels generally have a simple rectangular geometry, the physical or geometrical volume can be calculated in terms of channel dimensions, provided that the latter are accurately known. In this case, the two volumes (inert retention volume and geometrical volume) can be compared for self-consistency and thus for assurance that an accurate V^0 is available. (A very small difference, usually $< 1\%$, in the two volumes can be induced by edge effects [5].) Once V^0 is known, t^0 can be calculated by means of the simple relationship

$$V^0 = \dot{V} t^0 \qquad (1)$$

where $\dot{V}$ is the volumetric flow-rate of carrier liquid flowing through the channel.

Correspondence to: J. C. Giddings, Field-Flow Fractionation Research Center, Department of Chemistry, University of Utah, Salt Lake City, UT 84112, USA.

* Present address: Via Ugo de Carolis 83, 00136 Rome, Italy.

0021-9673/92/$05.00

The dual approach noted above for obtaining V^0 is commonly employed in sedimentation and thermal FFF. However, the dual strategy has several weaknesses when applied to flow FFF channels [3,4]. First, and most important, the low-molecular-mass components that are most often used to probe the void volume are small enough in molecular dimensions that they generally penetrate into the semipermeable membrane used for the accumulation wall. When the upper (or depletion) wall is permeable, as is usual, they can also partition into this wall. Thus, at worst, the non-retained component will be lost through the membrane and fail to appear at the detector and, at best, the component will be delayed by virtue of its partitioning into stagnant pore space which will yield an erroneous result. Losses through the membrane can be minimized by eliminating the cross-flow during void peak migration, but then the component is more likely to partition into the larger pores of the depletion wall. A void probe of larger molecular size can be used to avoid membrane partitioning, but the pore space of the depletion wall (usually consisting of a flat slab of frit with micrometer-sized pores) can still be readily penetrated unless very large probes are used. If one does proceed to micrometer-sized probes, then hydrodynamic lift forces will influence their retention. Also, any increase in the size of the probe molecule or particle will slow its diffusion and thus increase the run time necessary to obtain a sharp and meaningful void peak.

The geometrical volume of flow FFF channels is also subject to uncertainty. In addition to the error in volume associated with the small geometrical uncertainties common to most FFF channels, flow FFF systems are generally constructed with a compressible membrane used for the accumulation wall [3,4]. As this membrane is clamped in place beneath a spacer of well characterized thickness, the uncompressed portion of the membrane protrudes into the channel space, occupying some of the volume that would normally be part of the void volume. This protrusion reduces the channel thickness w (and thus V^0) as illustrated in Fig. 1. Unless the degree of compression is well characterized, the actual thickness of the channel will not be known and thus V^0 will be undetermined. The uncertainty introduced by membrane compression makes it desirable to use thin and relatively incompressible membranes wherever possible. Many commercial membranes (one exception is noted below) are, however, subject to considerable compression, making the geometrical V^0 difficult to ascertain.

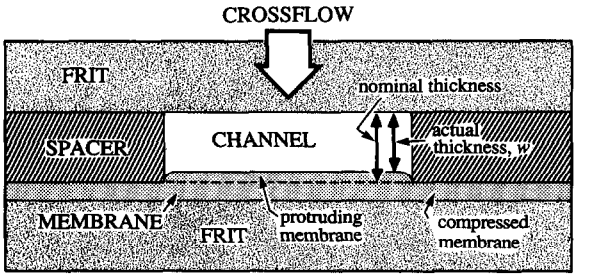

Fig. 1. Schematic cross-section (perpendicular to flow axis) of flow FFF channel showing effect of protruding membrane on channel thickness.

In order to improve void peak measurements in flow FFF (and perhaps also in other forms of FFF), it is useful to examine the flow profile over the channel thickness and its role in void peak transport. The flow profile is, of course, parabolic as illustrated in Fig. 2. Thus entrained molecules or particles will be carried along at a velocity $v(x)$ that differs from one position (expressed in terms of the distance x from the accumulation wall) to another along the transverse coordinate of the channel. If each molecule of a void probe stayed in its initial streamline, then the probe molecules would elute at widely different times because of their different velocities. In order to obtain a compact void peak, the flow velocity must be sufficiently slow that each probe molecule can diffuse numerous times across the channel in order to experience a statistical mix of all velocity vectors. However, this extended diffusion process, of necessity, brings the probe molecules to the channel walls where they may suffer unwanted retardation by the pores in the wall as described

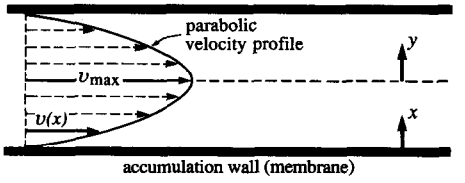

Fig. 2. Edge view of flow FFF channel showing parabolic flow velocity profile.

above. Hence the goals of obtaining a sharp and statistically meaningful void peak and of avoiding wall interactions are largely contradictory.

In view of the above contradiction, it is useful to examine the possibility of working at the other extreme where probe molecules have little opportunity for transverse diffusion before they are swept through the channel. In the limit of ultrafast flow or negligible diffusion, each probe will stay with its original streamline. The first probe molecules to appear will be those travelling at the centerline of the channel, which coincides with the apex of the parabola (see Fig. 2). In principle, the timing of these early arrivals, coupled with the assumption that the flow is parabolic, fully characterizes the fluid motion in the channel and the associated void time. This can be seen as follows.

The parabolic flow profile in an FFF channel with a rectangular cross-section of high aspect ratio can be expressed by [6]

$$v(x) = 6\langle v\rangle\left[\frac{x}{w} - \left(\frac{x}{w}\right)^2\right] \tag{2}$$

where $\langle v\rangle$ is the average cross-sectional velocity. At the center of the channel ($x/w = 0.5$), velocity v reaches a maximum value given by

$$v_{max} = \frac{3}{2}\langle v\rangle \tag{3}$$

This equation shows that the fastest probe molecules are traveling at a velocity 1.5 times greater than the average fluid velocity. Hence the time of first appearance, or breakthrough time t_b, of probe molecules will precede the void time t^0, which corresponds to the elution time of probe molecules sampling all streamlines, according to the relationship

$$t_b = \frac{2}{3}t^0 \tag{4}$$

Similarly, in view of the proportionality between time and volume, the measured breakthrough volume V_b will relate to V^0 according to

$$V_b = \frac{2}{3}V^0 \tag{5}$$

Thus, the measurement of t_b or V_b leads directly to the corresponding void parameter t^0 or V^0.

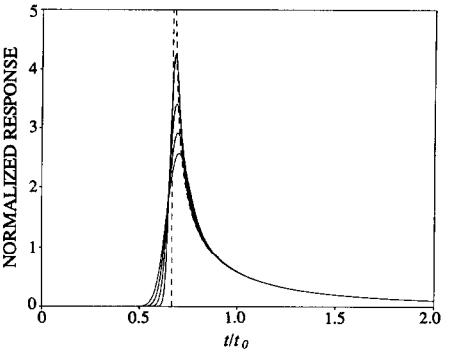

Fig. 3. Ideal peak profile (dashed curve) showing abrupt breakthrough in the zero diffusion limit, $\tau^0 \to 0$, and results of its convolution with Gaussian band spreading function for which $\sigma_t/t^0 = 0.02$, 0.03, 0.04 and 0.05.

We note that early peaks, eluting before t_0 or V^0, have been described previously in the FFF literature, but they have not been proposed as a means for determining V^0. "Leading peaks" resulting from incomplete relaxation in flow FFF were shown to precede V^0 in 1977 [7]. In discussing these peaks it was pointed out that non-diffusing particles traveling in the most rapid streamlines would elute after 67% of the void volume had been pumped into the channel. Similar peaks eluting prior to V^0 in sedimentation FFF were described in the early 1980s [8,9].

Ideally, the detector signal for a breakthrough peak will rise abruptly (see eqn. 11 and Fig. 3) at time $t = t_b$, thus giving an unequivocal measure of t_b. In practice, the abrupt rise is moderated by various non-idealities including longitudinal diffusion, finite detector response time, channel imperfections, channel end effects, finite sample size and peak broadening in the dead volume of inlet and outlet tubing and in the detector cell. We note that the dead volume must be subtracted from the experimental breakthrough volume to yield a meaningful V_b.

In addition, it is impossible to generate infinite flow-rates or to find probes with zero diffusivities to make this breakthrough procedure work perfectly. The criterion for workability, providing the above non-idealities are reduced to a minimum, can be formulated in terms of the dimensionless time given by

$$\tau = 4Dt/w^2 \tag{6}$$

where D is the diffusion coefficient of the probe material and t is the time elapsed from sample introduction. As the time required to diffuse from the center of the channel to one wall is given approximately by $t_D = w^2/8D$, the dimensionless time τ may be defined alternatively in the following terms:

$$\tau = t/2t_D \quad (7)$$

The dimensionless void time τ_0 is then given by

$$\tau^0 = \frac{4Dt^0}{w^2} = \frac{t^0}{2t_D} \quad (8)$$

This parameter is a convenient measure of the ability of probe molecules or particles to sample all stream velocities during migration through the channel. Effective sampling by means of multiple diffusive excursions requires that $\tau^0 \gg 1$. Our proposed method requires that τ^0 be kept small relative to unity such that excursions across streamlines are minimized rather than maximized. The most practical approach to achieving low τ^0 values involves the dual strategy of increasing the flow-rate in order to reduce t^0 and of choosing macromolecular or colloidal probes for which D is small.

In this study we utilize a number of proteins as probes. The diffusion coefficients and the t_D values for various proteins in a channel of typical thickness, $w = 254$ μm, are given in Table I. These t_D values range from about 2 to 11 min. These values would be four times less in a twofold thinner channel, $w = 127$ μm. Larger t_D values, if desired, could be readily obtained using colloidal latex (see later). There is no strict need for the probe material to be monodisperse and its diffusion coefficient need not be accurately known.

It is clear that the best results using the above approach will be obtained when $\tau^0 \ll 1$. However, the degree to which τ^0 must fall below unity in practice must be determined by further work. Our preliminary results (see below) suggest that τ^0 values up to 0.5, and possibly higher, can be used to obtain consistent V^0 values. We note that there are specific characteristics of the parabolic flow profile that make the criterion $\tau^0 \ll 1$ less demanding than might be expected. Specifically, the maximum of a parabolic flow profile is rather blunt, which means that a probe molecule starting at the channel centerline can diffuse a considerable fraction of channel thickness w before becoming entrained in low velocity streamlines. This is seen best by converting eqn. 2 to the form

$$\frac{v}{v_{max}} = 1 - \left(\frac{2y}{w}\right)^2 \quad (9)$$

where y (which replaces x) is the distance from the centerline (see Fig. 2). This can be rearranged to

$$\frac{2y}{w} = \left(1 - \frac{v}{v_{max}}\right)^{1/2} \quad (10)$$

Eqn. 10 can be utilized as follows. If we decide that the probe molecule must stay within a central lamina of such thickness ($2y$) that the flow velocity maintains at least 90% of its maximum velocity ($v/v_{max} = 0.9$), then eqn. 8 shows that the probe can undertake diffusive excursions that extend across almost 32% of the channel ($2y/w = 0.32$). If, more rigorously, we require that all stream velocities in the lamina be within 5% of the maximum, then $2y/w = 0.22$. A lamina containing only 1% velocity variation still leaves 10% of the channel available for diffusive displacement.

The fact that the velocity drops off only modestly as one moves away from the centerline is a great advantage to the present method of void volume determination. The first advantage, as implied above, is that probe molecules can undergo finite diffusional displacements without losing their value as breakthrough probes. Second, since the lamina in which flow velocities have only a negligible departure from

TABLE I

DIFFUSION COEFFICIENTS, D, AND DIFFUSION TIMES, $t_D = w^2/8D$, FOR SODIUM BENZOATE AND VARIOUS PROTEINS IN A 0.0254 cm THICK FFF CHANNEL AT 20°C

Probe	$D \cdot 10^7$ (cm^2/s)[a]	t_D (s)
Sodium benzoate	83.0	9.7
Ovalbumin	7.8	100
Hemoglobin	6.7	120
α-Globulin	5.2	160
γ-Globulin	4.0	200
Horse fibrinogen	1.2	670

[a] From *Handbook of Biochemistry* (CRC, 1978), except for sodium benzoate, for which D was taken from ref. 25.

the maximum velocity is fairly thick, it contains a substantial fraction of all the probe molecules initially introduced into the channel. This large breakthrough population, emerging almost simultaneously, will obviously simplify detection and measurement. More specifically, the sudden breakthrough will lead to an abrupt rise to a peak maximum in the detector signal $S(t/t^0)$, followed by a rapid drop and finally by a slowly attenuating tail representing the elution of probe molecules carried by the slower streamlines. It can be shown (see Appendix) that the ideal normalized peak profile (in the zero diffusion limit) is given by

$$S(t/t^0) = \frac{(t^0/t)^2}{(9 - 6t^0/t)^{1/2}} \tag{11}$$

which has unit area on the dimensionless time scale t/t^0. This function is valid for time $t > 2t^0/3$ and approaches infinity as $t \to 2t^0/3$. A plot of $S(t/t^0)$ is shown as a dashed line in Fig. 3.

The approach described here is equally applicable to the determination of the internal volumes of uniform straight tubes. In tubes of circular cross-section the velocity of fluid at the center line is twice the mean fluid velocity, which results in an ideal breakthrough time equal to half the void time. Ordinarily the tube should be straight because curvature gives rise to secondary flows, particularly important at high flow-rates. The secondary flows will mix the probe particles or molecules from the various regions of the tube cross-section. (Some weaker secondary flows will also be encountered in curved FFF channels.) Sampling of the various stream velocities by the probe species is thereby enhanced and the ideal sharp breakthrough curve degraded. (In order to counteract secondary flow effects in curved tubes the flow-rate would need to be limited, thus requiring that the probe species have an unusually low diffusion coefficient to keep τ_0 small.) This enhanced secondary mixing and that induced at transition points in the flow path explain why the full dead volume of connecting tubes and fittings, rather than some fraction of this dead volume, is subtracted from observed volumes in our determination of FFF channel void volumes.

The published literature concerning breakthrough curves for straight tubes of circular cross-section is far more extensive than for parallel-plate systems (see, *e.g.*, refs. 10–37). Studies were initiated by Taylor [10,11] and Aris [12], who derived the asymptotic solution for $\tau \gg 1$, where $\tau = Dt/R^2$ with R being the internal radius of the tube. Later studies were concerned mainly with the theoretical prediction and experimental observation of breakthrough curves at lower τ^0, where $\tau^0 = Dt^0/R^2$. The general behavior is well established. When $\tau^0 \ll 1$ the ideal normalized breakthrough curve for an eluted sample is described by (see Appendix)

$$S(t/t^0) = \frac{1}{2}\left(\frac{t^0}{t}\right)^2 \tag{12}$$

an equation valid when $t/t^0 > 1/2$. [We note that most studies to date have utilized on-tube detection which results in $S(t/t^0)$ decaying with $1/t$; see Caro [14] and Lighthill [15].] As τ^0 increases, the tail predicted by eqn. 12 becomes truncated because the longer residence time allows those sample components entrained in streamlines adjacent to the walls to diffuse into faster streams and elute earlier. This tendency is aided by the fact that the time for elution is greatest for these components and the shear rate of the carrier is greatest at the wall. The latter point tells us that if a particle or molecule moves a relatively small distance away from the wall it will encounter considerably faster fluid velocities. For $\tau^0 \approx 0.05$, a distinct shoulder appears on the trailing side of the breakthrough curve. For still larger τ^0, the curve takes on a bimodal form, provided system non-idealities do not mask the effect. The leading peak is due to the fast elution of material near the center of the tube and the trailing peak is due to material diffusing inward from the wall. The second peak tends to build close to the true void time as τ^0 increases. At $\tau^0 \approx 0.5$, the leading peak has a much reduced presence in the overall elution curve, and at $\tau^0 \approx 1$ the curve already is fairly well approximated by the predicted high τ asymptotic peak whose elution is centered about t^0.

Parallel-plate FFF systems are likely to exhibit a similar variation in breakthrough curve behavior at comparable dimensionless times. For instance, the effective longitudinal dispersion coefficient in tube flow was predicted [17] to reach a constant level at $\tau \approx 0.5$. In parallel-plate systems the dispersion coefficient is likewise predicted [38] to approach a constant value at $\tau \approx 0.5$. Monte Carlo simulations [39] of particle migrations in parallel-plate systems support qualitative similarity with tube flow sys-

tems. At $\tau^0 = 0.15$, the predicted breakthrough curve exhibits a sharp front and a shoulder on the trailing side. At $\tau^0 = 0.67$, a single peak was predicted with a maximum slightly preceding the theoretical void time. For intermediate τ^0, we might expect a gradual transformation which may or may not pass through a bimodal stage. The parallel-plate system results in a t_b of $2t^0/3$ as opposed to $t^0/2$ for tubular flow. The material eluting in the central region will not be as well separated from that which samples a wider range of velocity and elutes closer to t^0.

It is reasonable to suppose that provided $\tau^0 \lesssim 0.1$ for both parallel-plate and tube flow, the leading part of the breakthrough curve will correspond closely with the ideal $\tau^0 = 0$ curve. For our purposes we are not concerned with the form of the trailing portion of the elution curve.

It was mentioned earlier that, in practice, the abrupt rise in the ideal elution profile will be moderated by various non-idealities of the system. These non-idealities can be modeled by convoluting the ideal curve with a Gaussian function representing the combination of band spreading effects. The non-idealities will differ from system to system and we therefore expect the standard deviation (σ_t) for the Gaussian band spreading function to vary significantly between systems. Fig. 3 shows the results of convolution of the ideal curve for a parallel-plate system (dashed line) with Gaussian functions for which $\sigma_t/t^0 = 0.02, 0.03, 0.04$ and 0.05. As σ_t/t^0 increases, the initial rise is seen to become less steep and the peak maximum is displaced to higher t/t^0. Thus the breakthrough point becomes more difficult to identify. Fig. 3 shows that a significant error will be incurred if breakthrough is identified with the peak maximum. A still larger error will be found by equating the breakthrough time with the time of the initial observed rise of the signal. However, we observe that each of the convoluted curves appears to intersect the ideal vertical breakthrough (dashed) line found at $t/t^0 = 2/3$ at a fairly constant fraction of its maximum height. We may be able to exploit this property to determine void times and void volumes accurately even for non-ideal breakthrough curves.

To explore the above possibility in more detail, the ideal profile was convoluted with a set of Gaussian functions with σ_t/t^0 ranging from 0.004 to 0.10. The relative heights of the points of intersection with the ideal breakthrough line at $t/t^0 = 2/3$ were obtained. These are plotted in Fig. 4 as h_b/h_{max} *versus* σ_t/t^0, where h_b is the height of each curve at $t/t^0 = 2/3$ and h_{max} is the maximum height of each respective curve. The value of h_b/h_{max} increases from around 0.84 for $\sigma_t/t^0 = 0.004$ up to 0.88 at $\sigma_t/t^0 = 0.10$. Examination of typical elution profiles for non-retained, low-diffusing materials suggests that σ_t/t^0 is generally much less than 0.05 (see Figs. 3, 7, 8 and 9) and we can therefore assume that h_b/h_{max} will fall in the narrow range between 0.84 and 0.86.

The final objective, of course, is to determine the breakthrough value, $t_b = (2/3)t^0$, and hence t^0 and V^0. For small σ_t/t^0 the convoluted result differs from the ideal curve to only a small extent. The initial rise remains relatively steep and consequently the value deduced for t_b will be insensitive to the value assumed for h_b/h_{max}. Therefore, if we need to select a best overall value for h_b/h_{max} for some range of σ_t/t^0, we might expect that the favorable choice would correspond to h_b/h_{max} for the upper limit for the range of σ_t/t^0. Discrete values for h_b/h_{max} of 0.84, 0.85, 0.86, 0.87 and 0.88 were examined with regard to their accuracy in the determination of t_b, and hence t^0 and V^0. Fig. 5 shows the percentage error realized for each of these discrete values as σ_t/t^0 ranges from 0 to 0.1. As expected, if the range of interest for σ_t/t^0 extends to 0.10, then the best overall value for h_b/h_{max} is close to 0.88. If σ_t/t^0 is expected to lie below 0.05 (as we have suggested), then the best overall value will be close to 0.86. In the latter case the error in determination of void volume is pre-

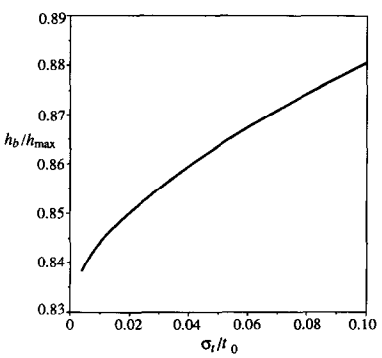

Fig. 4. Plot of h_b/h_{max} *versus* σ_t/t^0 of a Gaussian band spreading function convoluted with the ideal breakthrough curve.

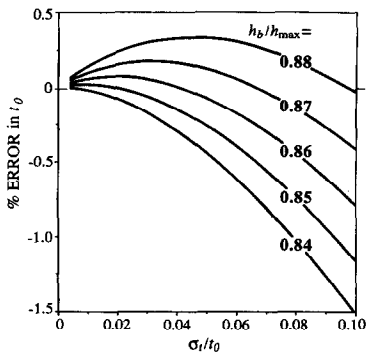

Fig. 5. Percentage error in determined t^0 as a function of σ_t/t^0 for band spreading function for each of the assumed values of h_b/h_{max}: 0.84, 0.85, 0.86, 0.87 and 0.88.

dicted to be less than 0.1% for any σ_t/t^0 less than 0.05.

Some of the experiments we report below involve the introduction of sodium benzoate as a relatively fast diffusing probe. For rapidly diffusing species the general long-time asymptotic solution obtained by Krishnamurthy and Subramanian [38] for an infinite parallel-plate system is expected to be applicable. This solution may be transformed to the following normalized function describing the predicted elution curve:

$$S(t/t^0) = \frac{t^0}{\sqrt{2\pi}\,\sigma_t}\left(\frac{t^0}{t}\right)^{1/2} \exp\left[-\frac{t^0}{t}\cdot\frac{(t^0-t)^2}{2\sigma_t^2}\right] \quad (13)$$

where

$$\sigma_t = w\left(\frac{t^0}{105D}\right)^{1/2} \quad (14)$$

Eqn. 13 requires only that $t^0D/w^2 \gg 1/8$ or $\tau^0 \gg 1/2$.

EXPERIMENTAL

Experimental measurements of void volumes were undertaken using four different channel structures. The channels were constructed by sandwiching a Teflon spacer between two wall elements. The volume cut out of the spacer constitutes the channel void volume. We designate the tip-to-tip length of the cutout section as L_{tt}, the thickness as w and the breadth as b.

To construct Channel I, the spacer was sandwiched between two transparent glass plates. The cutout dimensions are $L_{tt} = 22.5$, $w = 0.0254$ and $b = 2.0$ cm. The geometrical void volume is 0.99 ml (this is less than the product bwL_{tt} because the ends of the channel volume are tapered). Channel II is almost identical with Channel I ($L_{tt} = 22.0$, $b = 2.0$ cm) except that the spacer thickness w is 0.0127 cm and the geometrical V^0 is 0.48 ml.

Channel III is identical with Channel II except that a membrane was layered over the bottom glass wall. The membrane is Celgard 2400 from Hoechst-Celanese (Charlotte, NC, USA).

Channel IV is a conventional flow FFF channel [3,40] in which the walls are flat permeable frits. The bottom (accumulation) wall was covered by the Celgard 2400 membrane. In this case, $L_{tt} = 27.7$, $w = 0.0254$, $b = 2.0$ cm and the geometrical V^0 is 1.27 ml. For this channel, the inlet and outlet crossflow lines were joined together to prevent any displacement of liquid by crossflow during the run.

Each channel was connected by 0.787 mm I.D. tubing to an injection tee at the inlet end and the detector cell at the outlet. The inlet and outlet dead volumes were typically *ca.* 48 and *ca.* 62 μl, respectively.

Flow through the above channels was generated by an in-house syringe pump for most measurements and a Model 110B HPLC pump from Beckman Instruments (Berkeley, CA, USA) for the remaining measurements. The carrier liquid in all instances was 0.02% (w/w) sodium azide in doubly distilled, deionized water. Various proteins (listed in the tables) were used as the breakthrough probes. The proteins were complemented by a low-molecular-mass probe, sodium benzoate. All probes were injected by syringe into the inlet tubing next to the channel. The sample volumes injected were in the range 10–20 μl. The peaks were detected by a Model SPD-6A variable-wavelength detector from Shimadzu (Kyoto, Japan) with an 8-μl cell.

RESULTS AND DISCUSSION

All void volume determinations reported in Tables II–VI were based on the assumption that the sum of the dead time t_d and the breakthrough time t_b corresponds to the point on the elution curve front where $h = 0.86\,h_{max}$. Fig. 6 illustrates the interpreta-

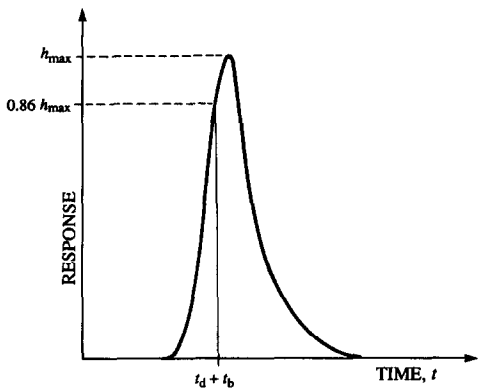

Fig. 6. Interpretation of elution curve for sample probe for which $\tau^0 < 0.1$.

tion of the elution curve for a sample probe for which $\tau^0 < 0.1$. A perpendicular is dropped to the time axis from a point on the front of the peak corresponding to 0.86 of the peak height h_{max}. The dead time t_d ($= V_d/\dot{V}$) is subtracted from the time recorded at the foot of the perpendicular to obtain the breakthrough time t_b. This subtraction is necessary because run time is measured from the time of sample injection. The void time t^0 is obtained from t_b simply by multiplying by 3/2, and the void volume is then given by eqn. 1. The reported V^0 values represent the means for several repeat runs, and standard deviations σ in V^0, where reported, were determined from a minimum of five such repeat runs. The dimensionless void times τ_0 in all tables were calculated according to nominal geometric channel dimensions.

TABLE II

VOID VOLUMES, V^0, WITH STANDARD DEVIATIONS, σ, DETERMINED FOR CHANNEL I (ASSUMING $h_b/h_{max} = 0.86$) WITH VARIOUS PROTEIN PROBES AT THE INDICATED FLOW-RATES AND DIMENSIONLESS VOID TIMES, τ^0, CALCULATED ACCORDING TO NOMINAL GEOMETRICAL DIMENSIONS

Probe	$\dot{V} = 0.55$ ml/min		$\dot{V} = 1.44$ ml/min		
	τ^0	V^0 (ml)	τ^0	V^0 (ml)	σ (ml)
Ovalbumin	0.52	1.02	0.20	1.00	0.018
Hemoglobin	0.45	1.02	0.17	0.98	–
α-Globulin	0.35	1.02	0.13	0.99	–
γ-Globulin	0.27	1.03	0.10	0.99	0.005
Horse fibrinogen	0.080	0.98	0.030	0.98	0.013

TABLE III

VOID VOLUMES, V^0, WITH STANDARD DEVIATIONS, σ, DETERMINED FOR CHANNEL II (ASSUMING $h_b/h_{max} = 0.86$) WITH VARIOUS PROTEIN PROBES AT $\dot{V} = 0.58$ ml/min AND VALUES FOR τ^0 CALCULATED ACCORDING TO NOMINAL DIMENSIONS

Probe	τ^0	V^0 (ml)	σ (ml)
Ovalbumin	0.96	0.65	0.012
Hemoglobin	0.83	0.63	0.024
γ-Globulin	0.49	0.53	0.044
Horse fibrinogen	0.15	0.45	0.019

The results for determination of V^0 for Channel I are listed in Table II. The protein probes were eluted at channel flow-rates $\dot{V}$ of 0.55 and 1.44 ml/min. The dead volume for the connecting tubing was calculated to be 0.105 ml. The overall agreement between the results is seen to be excellent, and all are close to the geometrical volume of 0.99 ml. Even the experiments with ovalbumin at $\dot{V} = 0.55$ ml/min, for which $\tau^0 = 0.52$, yield a value for V^0 in good agreement with determinations using more slowly diffusing probes. It appears that at least in this instance, where the channel has impermeable glass walls, the condition $\tau^0 \ll 1$ may be relaxed considerably.

Table III shows the results obtained for Channel II. In this instance both w and the geometrical volume (0.48 ml) are reduced by a factor of 2

TABLE IV

VOID VOLUMES, V^0, WITH STANDARD DEVIATIONS, σ, DETERMINED FOR CHANNEL II (ASSUMING $h_b/h_{max} = 0.86$) USING SODIUM BENZOATE AT THE INDICATED FLOW-RATES AND VALUES FOR τ^0 CALCULATED ACCORDING TO NOMINAL DIMENSIONS

$\dot{V}$ (ml/min)	τ^0	V^0 (ml)	σ (ml)
0.51	12.0	0.69	0.014
0.97	6.1	0.66	0.021
4.24	1.4	0.57	0.013

compared with Channel I. The dead volume was calculated to be 0.100 ml. Any uncertainty in the dead volume will therefore have a larger influence on the accuracy of determined V^0 values for Channel II than for Channel I. Horse fibrinogen, for which $\tau^0 = 0.15$ at $\dot{V} = 0.58$ ml/min, yields a value for V^0 of 0.45 ml, which is close to the geometrical volume. The result for γ-globulin is slightly higher at 0.53 ml, which is reasonable even though $\tau^0 = 0.49$. Hemoglobin and ovalbumin yield still higher V^0 values, as expected considering the relatively high τ^0 for these runs. (The high τ^0 values are a consequence of the reduced channel thickness w. These τ^0 values could be reduced and accuracy improved by using more slowly diffusing probes, as explained later.)

Sodium benzoate was also introduced as a probe for Channel II. Three flow-rates, 0.51, 0.97 and 4.24 ml/min, were employed for which $\tau^0 = 12.0$, 6.1 and 1.4, respectively. The results for the determination of V^0, using the method employed for protein probes, are given in Table IV. The V^0 values determined in this way are higher than the true V^0, as expected for $\tau^0 > 1$. We note that as τ_0 is allowed to increase, the peak maximum (when adjusted for the dead time $t_d = V_d/\dot{V}$, where V_d is the total dead volume) is expected to approach the void time t^0 (see eqn. 13). The relative width of the elution peak will at the same time decrease because molecules have more time to sample all stream velocities. This effect is apparent by rearranging eqn. 14 as follows:

$$\frac{\sigma_t}{t^0} = \frac{w}{(105t^0D)^{1/2}} = \frac{2}{(105\tau^0)^{1/2}} \quad (15)$$

The net result is that the point corresponding to 0.86 h_{max} will approach t^0 (corrected for t_d) for large τ^0, rather than $(2/3)t^0$ as expected for small τ^0. The assumption of high τ^0 behavior would yield V^0 values equal to two third of the volumes listed in Table IV. For example, the experiments corresponding to $\tau^0 = 12$ would yield $V^0 = 0.46$ ml if high τ^0 asymptotic behavior is assumed. This value of 0.46 ml is in good agreement with the result obtained at small τ^0 with horse fibrinogen, 0.45 ml, and is close to the geometrical volume of 0.48 ml. The highest flow-rate, for which $\tau^0 = 1.4$, yields a value of $V^0 = 0.57$ ml (assuming low τ^0 behavior with $h_b/h_{max} = 0.86$). This is higher than the probable true value for V^0 and lower than the value obtained for $\tau^0 = 12.0$, which suggests intermediate behavior in which both diffusion and convection contribute significantly to transport. Such intermediate behavior, although of theoretical interest, is clearly not desirable for void volume determinations.

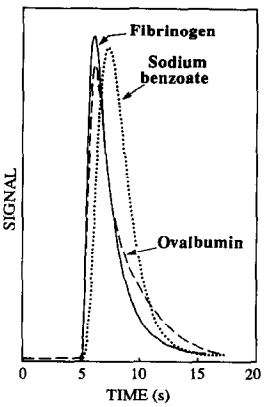

Fig. 7. Elution profiles for fibrinogen, ovalbumin and sodium benzoate sample probes injected into Channel III at a flow-rate $\dot{V}$ of 4.18 ml/min.

Fig. 7 shows typical overlayed elution curves for horse fibrinogen, ovalbumin and sodium benzoate samples injected into Channel III with a flow-rate of 4.18 ml/min. The τ^0 values were calculated to be 0.021, 0.13 and 1.4, respectively. The protein probes yield peaks that rise sharply at the front and then tail. The tails are not as extended as predicted by the plots for $\tau^0 = 0$ shown in Fig. 3. This is expected, as we explained earlier, since material will diffuse out of the regions close to the walls into faster fluid streams. The fibrinogen and ovalbumin peaks yield V^0 values of 0.45 and 0.46 ml, respectively, based on the breakthrough approach. The peak for sodium benzoate is more symmetrical and the peak maximum is retarded relative to the others. The low τ^0 breakthrough approach yields $V^0 = 0.57$ ml while the high τ^0 peak maximum approach yields $V^0 = 0.42$ ml. The former value is in good agreement with the result obtained for Channel II with sodium benzoate at $\tau^0 = 1.4$. Again, this suggests intermediate behavior since the results bracket the probable true V^0.

In Fig. 8 we show typical overlayed elution curves for horse fibrinogen, hemoglobin and sodium benzoate injected into Channel III once more, but at a reduced flow-rate of 0.55 ml/min. The τ^0 values are

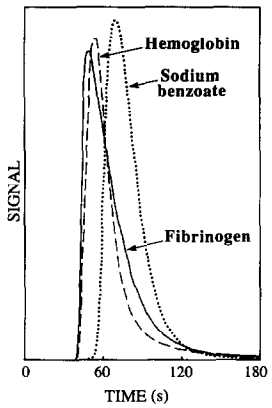

Fig. 8. Peak profiles for fibrinogen, hemoglobin and sodium benzoate in Channel III with $\dot{V} = 0.55$ ml/min.

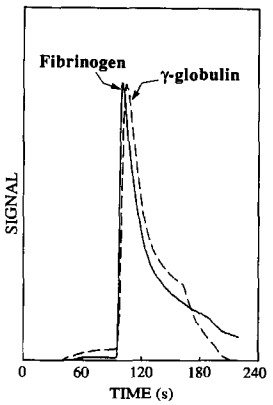

Fig. 9. Breakthrough profiles for fibrinogen and γ-globulin eluted from flow FFF channel (Channel IV) at $\dot{V} = 0.58$ ml/min.

increased relative to those in Fig. 7 by a factor of *ca.* 8, being 0.16, 0.87 and 11.0, respectively. The peak for fibrinogen rises abruptly as with the higher flow-rate, but that for hemoglobin is apparently influenced by the diffusive component to transport. The rise is less abrupt and the peak maximum is slightly retarded. The peak for sodium benzoate is more symmetric and relatively narrower than that obtained at the higher flow-rate. The reduction in relative peak width is in agreement with the prediction of eqn. 15. The dead volume of 0.103 ml (applicable to this channel) requires subtraction of a dead time t_d of 11 s. The benzoate peak maximum, eluting at 68 s, yields a void time of 57 s and thus a void volume of 0.52 ml (assuming high τ^0 behavior). Fibrinogen, on the other hand, yields a void volume of 0.46 ml (assuming low τ^0 behavior), in excellent agreement with results obtained at two other flow-rates as reported in Table V. The higher apparent V^0 for sodium benzoate may reflect diffusion into stationary fluid in membrane pores. The void volumes for Channel III determined with other protein probes at flow-rates of 1.42 and 4.18 ml/min are also given in Table V. The consistency of the results lends credence to our approach. The experimental void volume is determined to be 0.46 ml, which is just slightly smaller than the geometrical volume of 0.48 ml. The polypropylene membrane (Celgard 2400) used in this channel has an uncompressed thickness of only 25 μm. About 5 μm compression, with consequent protrusion of the uncompressed membrane into the channel, would be required to

TABLE V

VOID VOLUMES, V^0, WITH STANDARD DEVIATIONS, σ, DETERMINED FOR CHANNEL III (ASSUMING $h_b/h_{max} = 0.86$) WITH VARIOUS PROTEIN PROBES AT THE TWO INDICATED FLOW-RATES AND VALUES FOR τ^0 CALCULATED ACCORDING TO NOMINAL DIMENSIONS

Probe	$\dot{V} = 1.42$ ml/min			$\dot{V} = 4.18$ ml/min		
	τ^0	V^0 (ml)	σ (ml)	τ^0	V^0 (ml)	σ (ml)
Ovalbumin	0.39	0.47	0.007	0.13	0.46	0.004
Hemoglobin	—	—	—	0.11	0.47	0.009
γ-Globulin	0.20	0.46	0.006	0.068	0.45	0.012
Horse fibrinogen	0.060	0.46	0.005	0.021	0.46	0.004

TABLE VI

VOID VOLUMES, V^0, WITH STANDARD DEVIATIONS, σ, DETERMINED FOR CHANNEL IV (ASSUMING $h_b/h_{max} = 0.86$) WITH VARIOUS PROTEIN PROBES AT $\dot{V} = 0.58$ ml/min AND VALUES FOR τ^0 CALCULATED ACCORDING TO NOMINAL DIMENSIONS

Probe	τ^0	V^0 (ml)	σ (ml)
Ovalbumin	0.64	1.31	–
α-Globulin	0.42	1.30	0.016
γ-Globulin	0.33	1.31	0.009
Horse fibrinogen	0.098	1.28	0.017

explain the difference. However, small uncertainties in channel breadth, dead volume effects, etc., may contribute to the small discrepancy.

Overlayed elution curves for horse fibrinogen and γ-globulin obtained with Channel IV at a flow-rate of 0.58 ml/min are shown in Fig. 9. The τ^0 values were calculated to be 0.098 and 0.33, respectively. The peaks are seen to rise abruptly, as observed in the previous cases. However, the trailing edges of the peaks are drawn out and distorted, probably owing to the diffusion of protein into the pores of the frits. Although the trailing edges of the peaks may be distorted by the porous walls, the leading edges appear (and according to theory should be) normal as a consequence of the fact that protein molecules starting near the channel centerline do not have sufficient time during the run to reach the walls and engage in partitioning into the pores. Void volumes determined for Channel IV with protein probes at a flow-rate of 0.58 ml/min are listed in Table VI. The agreement of the average experimental V^0 of 1.30 ml with the geometrical volume of 1.27 ml is fairly good. This suggests that the thin polypropylene (Celgard 2400) membrane does not give rise to significant compressibility problems associated with some ultrafiltration membranes that have been used in flow FFF systems [3,4].

CONCLUSIONS

The results of this study demonstrate that the void volume of FFF-like channels can be measured with reasonable consistency and accuracy based on the breakthrough time of a probe component that undergoes minimal transverse diffusion during elution. The constraint on diffusion is given by $\tau^0 \ll 1$, where τ_0 is the dimensionless ratio of the void time to twice the diffusion time as given by eqn. 8. The criterion $\tau^0 \ll 1$ can be fulfilled by using high flow-rates and/or probes with low diffusion coefficients (in more concrete and practical terms, this criterion can be stated as $\tau^0 < 0.1$).

In the studies reported we used a variety of protein molecules as probes because these high-molecular-mass components have low diffusion coefficients, in the range 10^{-6}–10^{-7} cm^2/s. For these probes in a typical 254-μm thick channel, the diffusion time is roughly 1–10 min. The requirement that $\tau^0 \ll 1$ therefore means that the void time t^0 and the breakthrough time t_b should be much smaller than these diffusion times, thus being forced down to values in extreme cases of no more than a few seconds. Although some of our results were obtained in this time frame and showed reasonable consistency, it is likely that better results could be obtained for most experimental systems (including our own) employing longer experimental times that would be less disturbed by various time constants of the system and small errors in the measurement of injection time and breakthrough time. The demand for such high-speed measurement could be most simply relaxed by using probes of even lower diffusivity. Perhaps most suitable would be polystyrene latex beads, which are available in a great range of sizes above 0.1 μm diameter. For example, a latex bead of diameter 0.436 μm at 25°C has a diffusion coefficient $D = 1.00 \cdot 10^{-8}$ cm^2/s, which is from one to two orders of magnitude less than the D values of the proteins used in this study. As shown by eqn. 8, the smaller D would allow (but not require) an increase by the same factor in t^0 without violating the condition $\tau^0 \ll 1$.

The optimum size of latex void probes would have to be established by additional experiments. We note that above *ca.* 0.5 μm diameter, hydrodynamic lift forces begin to play an important role in particle transport along the transverse axis of the channel [41]. These forces exert the greatest influence on particles close to the channel walls but, in principle, because of channel symmetry, do not disturb the trajectories of particles at the channel centerline that generate the breakthrough signal. Hence whereas lift forces may significantly alter the ideal elution profile

of Fig. 3, they may have little influence on the validity of breakthrough measurements. It may therefore be possible to use breakthrough probes exceeding 1 μm diameter. Whether or not this is actually feasible and whether there is any practical advantage of such large probes over submicrometer-size latex probes can only be answered by further experimentation.

SYMBOLS

b	Channel breadth
D	Diffusion coefficient
h_b	Height of void peak at $t = t_b$
h_{max}	Maximum height of void peak
L_{tt}	Tip-to-tip channel length
r	Radial distance from tube center
R	Internal tube radius
$S(t/t^0)$	Detector signal as function of t/t^0
t	Time
t_b	Breakthrough time
t_d	Dead time ($= V_d/\dot{V}$)
t_D	Diffusion time
t^0	Channel void time
$\langle v \rangle$	Mean fluid velocity
v_{max}	Maximum fluid velocity
$v(x)$	Velocity of flow vector at position x
$\dot{V}$	Channel flow-rate
V_b	Breakthrough volume
V_d	Dead volume
V^0	Channel void volume
w	Channel thickness
x	Distance from accumulation wall
y	Distance from channel centerline
σ_t	Standard deviation of Gaussian band spreading function
τ	Dimensionless time ($= 4Dt/w^2$ for parallel-plate systems, or Dt/R^2 for circular tubes)
τ^0	Dimensionless void time ($= 4Dt^0/w^2$ for parallel-plate systems, or Dt^0/R^2 for circular tubes)

ACKNOWLEDGEMENTS

This work was supported by Public Health Service Grant GM10851-35 from the National Institutes of Health. Supplementary support was provided by the industrially suponsored Technology Transfer Program of the Field-Flow Fractionation Research Center.

APPENDIX

A derivation of the ideal response curve for a non-retained pulse input to a parallel-plate channel, assuming negligible diffusion, is given below. In this derivation it is assumed that the sample is initially evenly distributed across the channel thickness, that the sample molecules do not migrate in a direction perpendicular to flow (by diffusion or any other means) and that the velocity of each molecule corresponds to that of the fluid occupying the same position relative to the walls. The ideal response assumes linear detector response and does not include any contribution to band spreading due to extra-channel effects.

The detector will respond to the mass per unit volume (or concentration) of solute eluted from the channel outlet. When the channel flow-rate is constant this will be proportional to the mass eluted per unit time. The elution time t for an element of fluid at a position x/w is given by

$$t = \frac{L}{v(x/w)} = \frac{L}{6\langle v \rangle \frac{x}{w}\left(1 - \frac{x}{w}\right)} \tag{A1}$$

where L is the channel length. From eqn. A1 it may be shown that

$$\left| \frac{dx/w}{dt} \right| = \frac{t^0}{6t^2\left(1 - \frac{2t^0}{3t}\right)^{1/2}} \tag{A2}$$

where it is required that $t > (2/3)t^0$.

The response therefore has the following proportionality:

$$\text{detector response} \propto \frac{\delta m}{\delta t} = \frac{\delta m}{\delta(x/w)} \left| \frac{\delta(x/w)}{\delta t} \right| \tag{A3}$$

where δm is the small element of mass that elutes in the small time interval δt, and as the sample is assumed to be uniformly distributed across the channel thickness, *i.e.*, $\delta m/\delta(x/w)$ must be constant, it follows that in the limit of $\delta t \to 0$ we have

$$\text{detector response} \propto \left| \frac{d(x/w)}{dt} \right| \tag{A4}$$

For convenience the response may be normalized to unit area for the dimensionless time scale of t/t^0. We obtain

$$S(t/t^0) = \frac{(t^0/t)^2}{(9 - 6t^0/t)^{1/2}} \tag{A5}$$

where $S(t/t^0)$ is the normalized response and it is again required that $t/t^0 > 2/3$.

The ideal response for a non-retained pulse input to a straight tube of circular cross-section is derived similarly. The elution time t for an element of fluid at a radial distance r from the center of the tube is given by

$$t = \frac{L}{v(r/R)} = \frac{L}{2\langle v\rangle\left[1 - \left(\frac{r}{R}\right)^2\right]} \tag{A6}$$

where R is the internal radius of the tube and L is its length. From eqn. A6 we see that for $t > t^0/2$

$$\frac{dr/R}{dt} = \frac{t^0}{4t^2\left(1 - \frac{t^0}{2t}\right)^{1/2}} \tag{A7}$$

In the case of an input pulse uniformly distributed across the tube cross-section, we have $\delta m/\delta(r/R) \propto r/R = [1 - t^0/(2t)]^{1/2}$. It follows that for elution of the sample from the tube

$$\text{detector response} \propto \frac{t^0}{4t^2} \tag{A8}$$

Normalizing this result to unit area on the t/t^0 scale, we obtain

$$S(t/t^0) = \frac{1}{2}\left(\frac{t^0}{t}\right)^2 \tag{A9}$$

where it is required that $t/t^0 > 1/2$. For $t/t^0 \leqslant 1/2$, $S(t/t^0) = 0$.

REFERENCES

1 J. C. Giddings, G. C. Lin and M. N. Myers, *J. Colloid Interface Sci.*, 65 (1978) 67.
2 J. C. Giddings, G. C. Lin and M. N. Myers, *J. Liq. Chromatogr.*, 1 (1978) 1.
3 S. K. Ratanathanawongs and J. C. Giddings, in T. Provder (Editor), *Particle Size Distribution II: Assessment and Characterization (ACS Symposium Series*, No. 472), American Chemical Society, Washington, DC, 1991, Ch. 15.
4 J. C. Giddings, S. K. Ratanathanawongs, B. N. Barman, M. H. Moon, G. Liu, B. L. Tjelta and M. E. Hansen, in H. Bergna (Editor), *Colloid Chemistry of Silica (Advances in Chemistry Series*, No. 234), American Chemical Society, Washington, DC, in press.
5 J. C. Giddings and M. R. Schure, *Chem. Eng. Sci.*, 42 (1987) 1471.
6 J. C. Giddings, *Unified Separation Science*, Wiley, New York, 1991.
7 F. J. Yang, M. N. Myers and J. C. Giddings, *Anal. Chem.*, 49 (1977) 659.
8 J. J. Kirkland, W. W. Yau, W. A. Doerner and J. W. Grant, *Anal. Chem.*, 52 (1980) 1944.
9 C. H. Dilks, Jr., W. W. Yau and J. J. Kirkland, *J. Chromatogr.*, 315 (1984) 45.
10 G. Taylor, *Proc. R. Soc. London, Ser. A*, 219 (1953) 186.
11 G. Taylor, *Proc. R. Soc. London, Ser. A*, 225 (1954) 473.
12 R. Aris, *Proc. R. Soc. London, Ser. A*, 235 (1956) 67.
13 H. R. Bailey and W. B. Gogarty, *Proc. R. Soc. London, Ser. A*, 269 (1962) 352.
14 C. G. Caro, *J. Physiol.*, 185 (1966) 501.
15 M. J. Lighthill, *J. Inst. Math. Its Appl.*, 2 (1966) 97.
16 V. Ananthakrishnan, W. N. Gill and A. J. Barduhn, *AIChE J.*, 11 (1965) 1063.
17 W. N. Gill and V. Ananthakrishnan, *AIChE J.*, 13 (1967) 801.
18 W. N. Gill and R. Sankarasubramanian, *Proc. R. Soc. London, Ser. A*, 316 (1970) 341.
19 W. N. Gill and R. Sankarasubramanian, *Proc. R. Soc. London, Ser. A*, 322 (1971) 101.
20 H. Bate, S. Rowlands, J. A. Sirs and H. W. Thomas, *Br. J. Appl. Phys. (J. Phys. D)*, 2 (1969) 1447.
21 J. S. Yu, *J. Appl. Mech.*, 43 (1976) 537.
22 J. S. Yu, *J. Appl. Mech.*, 46 (1979) 750.
23 W. N. Gill and R. S. Subramanian, *J. Appl. Mech.*, 47 (1980) 975.
24 J. S. Yu, *J. Appl. Mech.*, 48 (1981) 217.
25 M. J. E. Golay and J. G. Atwood, *J. Chromatogr.*, 186 (1979) 353.
26 J. G. Atwood and M. J. E. Golay, *J. Chromatogr.*, 218 (1981) 97.
27 K. P. Mayock, J. M. Tarbell and J. L. Duda, *Sep. Sci. Technol.*, 15 (1980) 1285.
28 B. Andersson and T. Berglin, *Proc. R. Soc. London, Ser. A*, 377 (1981) 251.
29 J. T. Vanderslice, K. K. Stewart, A. G. Rosenfeld and D. J. Higgs, *Talanta*, 28 (1981) 11.
30 J. E. Houseworth, *J. Fluid Mech.*, 142 (1984) 289.
31 C. N. Trumbore, M. Grehlinger, M. Stowe and F. M. Kelleher, *J. Chromatogr.*, 322 (1985) 443.
32 S. C. Chikwendu, *Int. J. Eng. Sci.*, 24 (1986) 1031.
33 J. S. Vrentas and C. M. Vrentas, *AIChE J.*, 34 (1988) 1423.
34 T. Korenaga, F.-H. Shen, H. Yoshida and T. Takahashi, *Anal. Chim. Acta*, 214 (1988) 97.
35 T. Korenaga, F. Shen and T. Takahashi, *AIChE J.*, 34 (1989) 1395.
36 A. Shankar and A. M. Lenhoff, *AIChE J.*, 35 (1989) 2048.
37 A. Shankar and A. M. Lenhoff, *J. Chromatogr.*, 556 (1991) 235.
38 S. Krishnamurthy and R. S. Subramanian, *Sep. Sci.*, 12 (1977) 347.
39 M. R. Schure, *Anal. Chem.*, 60 (1988) 1109.
40 J. C. Giddings, M. N. Myers, K. D. Caldwell and S. R. Fisher, *Methods Biochem. Anal.*, 26 (1980) 79.
41 P. S. Williams, T. Koch and J. C. Giddings, *Chem. Eng. Commun.*, 111 (1992) 121.